Journal of Membrane Science 372 (2011) 210–218

Contents lists available at ScienceDirect

Journal of Membrane Science

journal homepage: www.elsevier.com/locate/memsci

Fouling behavior of microstructured hollow fibers in cross-flow filtrations: Critical flux determination and direct visual observation of particle deposition

P.Z. Çulfaz[a,c], M. Haddad[a], M. Wessling[b,c], R.G.H. Lammertink[a,*]

[a] Soft Matter, Fluidics and Interfaces, Mesa+ Institute for Nanotechnology, University of Twente, PB 217, 7500AE Enschede, Netherlands
[b] Chemical Process Engineering, AVT, RWTH Aachen University, Turmstr. 46, 52056 Aachen, Germany
[c] Membrane Technology Group, University of Twente, PB 217, 7500AE Enschede, Netherlands

ARTICLE INFO

Article history:
Received 18 October 2010
Received in revised form 2 February 2011
Accepted 2 February 2011
Available online 4 March 2011

Keywords:
Microstructured membrane
Crossflow
Concentration polarization
Fouling
Yeast
Colloidal silica

ABSTRACT

The fouling behavior of microstructured hollow fiber membranes was investigated in cross-flow filtrations of colloidal silica and yeast. In addition to the as-fabricated microstructured fibers, twisted fibers made by twisting the microstructured fibers around their own axes were tested and compared to round fibers. In silica filtrations, the three different fibers showed similar behavior and increasing Reynolds number increased the critical fluxes significantly. In yeast filtrations, the twisted fiber performed similar to the round fiber and better than the structured fiber. Among the three fibers, during yeast filtrations the critical flux for irreversibility was highest for the twisted fiber. The Reynolds number had little effect on the critical fluxes for particle deposition, which was attributed to the strong adsorption of yeast particles on the membrane. On the other hand, the critical fluxes for irreversibility increased with increasing Reynolds number for all three fibers. Direct visual observation of yeast particles on the surface of the three different hollow fibers revealed that for the structured and twisted fibers, the initial deposition rate on the fins is much lower than that in the grooves. This is attributed to the shear-induced migration of the yeast particles from areas of high shear (fins) to those of low shear (grooves). Furthermore, on the fins of the twisted fiber the deposition rate was lower than that on the fins of the structured fiber. This observation, together with the observed high critical fluxes for the twisted fiber led to the conclusion that the twisting induces a secondary flow in the liquid. This secondary flow is effective in depolarizing the buildup of micron-sized yeast particles since the diffusion of these particles is strongly effected by gradients in shear rate. On the other hand, for the silica colloids which are much smaller, shear-induced diffusion is not significant and twisting does not have an improving effect on filtration.

1. Introduction

The performance of pressure-driven membrane processes for liquid-phase separations is adversely effected by concentration polarization and subsequent membrane fouling. Membrane fouling is one of the most important problems in a membrane process as it increases operational costs and reduces membrane lifetime. There are two main approaches to mitigate membrane fouling. By suitable choice of the membrane material or modification of the membrane surface, the adsorption of foulants on the membrane can be minimized [1,2]. However, this approach by itself is not enough to prevent fouling. Even though a membrane may be repulsive to potential foulants, retained material will still accumulate near the membrane and form a concentration polarization layer which can initiate the formation of a cake or gel layer [3]. The extent of concentration polarization and cake/gel formation ultimately depends on the balance between attractive and repulsive surface interactions of the filtered material, which is determined by the material's properties (e.g. size, surface charge), solution properties (e.g. pH, ionic strength, concentration) and the hydrodynamics (e.g. permeation rate, pressure, cross-flow velocity, shear rate) [1,4]. The latter can be modified such that concentration polarization is alleviated and cake or gel formation is prevented.

By applying cross-flow over the membrane, part of the foulant that would otherwise build up on the membrane can be swept away. Laminar flow decreases concentration polarization and compared to dead-end operation it becomes possible to carry out filtrations for extended periods without performance loss. Turbulent flow is more effective in diminishing the concentration polarization layer and preventing fouling and therefore enables the use of higher permeate fluxes. However the energy consumption is much higher than for laminar flow. To make use of the mixing effect of turbulence in disrupting concentration polarization layers without bringing about a high energy input, several approaches have

* Corresponding author. Tel.: +31 53 4892063; fax: +31 53 4894611.
E-mail address: r.g.h.lammertink@utwente.nl (R.G.H. Lammertink).

0376-7388/$ – see front matter © 2011 Elsevier B.V. All rights reserved.
doi:10.1016/j.memsci.2011.02.002

been suggested, such as the use of turbulence promoters [5], two-phase flow [6], pulsatile flow [7], corrugated membranes [8–12] and curvature-induced fluid instabilities [13–16].

A number of studies in literature have shown that introducing corrugations that lie normal to the feed flow direction on flat sheet membranes can promote turbulence and reduce concentration polarization significantly [8–12]. Apart from corrugated surfaces and turbulence promoting structures, turbulence can be passively created by curvature as well. Dean vortices, which are centrifugal instabilities formed in curved ducts, have been shown to depolarize foulant buildup during microfiltration and ultrafiltration in spiral, coiled, meander-shaped and helically twisted tubes or channels [13–16]. Broussous et al. fabricated ceramic tubular membranes with helical grooves on the inner surface and observed significant flux improvement compared to tubular membranes with smooth walls. They attributed this improved fouling performance to the flow disturbance by the helical structure [17,18].

In a previous study, we reported the fabrication of hollow fiber ultrafiltration membranes with microstructured outer surfaces. We showed that these membranes can be fabricated with the same intrinsic properties as round fibers fabricated under the same conditions. Therefore, they enable the same separation, and due to the microstructured surface they can offer enhanced productivity [19]. In this study, we investigate the fouling performance of these microstructured fibers in cross-flow filtrations. Additionally, by twisting the microstructured fibers around their axis we investigate the effect of having helical grooves that lie at an angle to the feed flow on the particle deposition. We use a flux-cycling method to determine the critical flux and direct visual observation to observe the deposition of yeast particles on the surface of the membranes (Fig. 1). Both straight and twisted microstructured fibers are compared to round fibers with the same intrinsic properties.

2. Experimental

2.1. Membranes and modules

The structured and round fibers used were made by the dry–wet phase inversion of the polymer dope 16.68% PES, 4.91% PVP K30, 4.91% PVP K90, 7.18% H_2O, 66.32% NMP, with water as the external coagulant. Details of the fabrication can be found elsewhere [19]. The structured fiber has 60% higher surface area per length compared to the round fiber (Fig. 2(a) and (b)). The pure water permeability of the fibers are 235 ± 11 L/h m^2 bar and 233 ± 12 L/h m^2 bar for structured and round fibers, respectively. The mean pore diameter of both fibers was found to be 12 nm by permporometry measurements. In addition to the structured fibers, twisted fibers were made by twisting each structured fiber around its own axis with about one full turn in 5 cm. The twisting was done after fabrication, when the fibers were dry. The pure water permeability and the pore size distribution remain unchanged after twisting. For flux-cycling experiments single-fiber modules of 40 cm length were prepared in 3 mm inner-diameter tubes. For direct visual observation (DVO), a flowcell made of three transparent PMMA plates was used. The plates were held together by a steel jacket and O-rings were placed between them to prevent leakage. The top plate was 2 mm thick, while the bottom and middle plates were 1 cm thick. The middle plate had an opening of 3 cm × 18 cm in the middle, and three 6-mm diameter holes on the two ends for potting the fibers. 6 mm outer-diameter tubes were glued into these holes in the middle plate to pot the fibers and extract the permeate. Three fibers were placed with equal spacing in the flowcell. A schematic of the middle plate of the flowcell is given in Fig. 2(c).

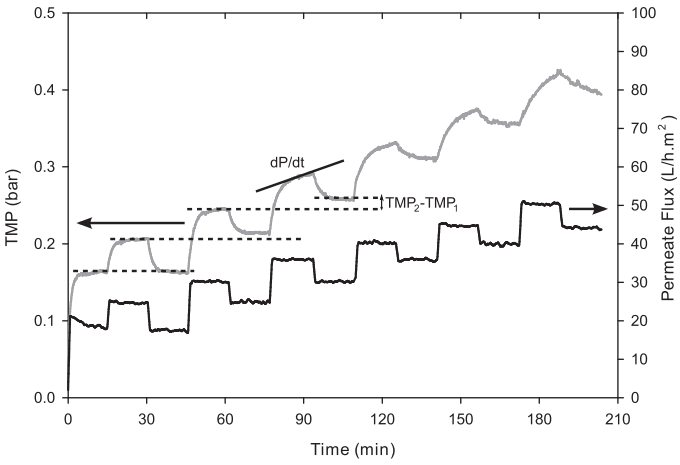

Fig. 1. Example of TMP-flux behavior and the calculation of the fouling rate and degree of irreversibility.

2.2. Flux-cycling experiments

0.25 wt% Ludox-TMA colloidal silica (Sigma–Aldrich) and 0.025 wt% Baker's yeast, *Saccharomyces cerevisiae*, (dry active yeast of Dr. Oetker) was used as feed suspensions. The as-purchased yeast was washed, filtered and dried overnight under air flow before preparing the feed suspensions. A fresh feed suspension was prepared for each experiment.

Before each experiment the pure water permeability of the membranes was measured as a check of membrane integrity.

To determine the critical flux, a flux-cycling method was used (Fig. 1) [20–22]. Flux steps of 5 L/h m^2 were applied, each step lasting 15 min. Two critical fluxes were defined, one with respect to the onset of particle deposition and the other one regarding the reversibility of this deposition [23]. To determine the critical flux for particle deposition, the evolution of TMP at constant flux during upward flux steps was monitored. The slope of the TMP during the last five minutes of the flux step, where the increase of TMP was linear, was calculated and plotted as dP/dt versus permeate flux. The flux where dP/dt becomes nonzero was taken as the critical flux for particle deposition. The degree of fouling reversibility was assessed by comparing the TMP's at the same flux on the way up and down (Fig. 1). For example, if the TMP on the way down is higher than that on the way up at 40 L/h m^2, then the critical flux for irreversibility was taken as 45 L/h m^2, as this is the flux step that caused irreversible deposition.

Each experiment was conducted twice for the determination of the critical flux. The first of these experiments was stopped after reaching the critical flux, while the second was continued further in order to determine the rate of particle deposition (dP/dt) and the degree of fouling reversibility (TMP_2–TMP_1) after the critical flux. The experiments were done under laminar conditions with Reynolds numbers of 120 and 400. $Re = 120$ corresponds to average cross flow velocities of 0.09 m/s for the structured and twisted fibers and 0.08 m/s for the round fiber. At $Re = 400$, the cross flow velocity was 0.31 m/s for the structured and twisted fibers and 0.27 m/s for the round fiber.

The flux-cycling experiments were carried out in the setup shown in Fig. 2(d). In this setup, the flowrates of feed and permeate as well as the pressures on the feed and permeate sides were logged every 5 s on a computer. The pressure on the retentate side was measured at the end of each experiment to calculate the TMP taking into account the pressure drop along the module length. When the yeast suspension was used as the feed, the suspension was stirred mildly during the course of the experiment to prevent

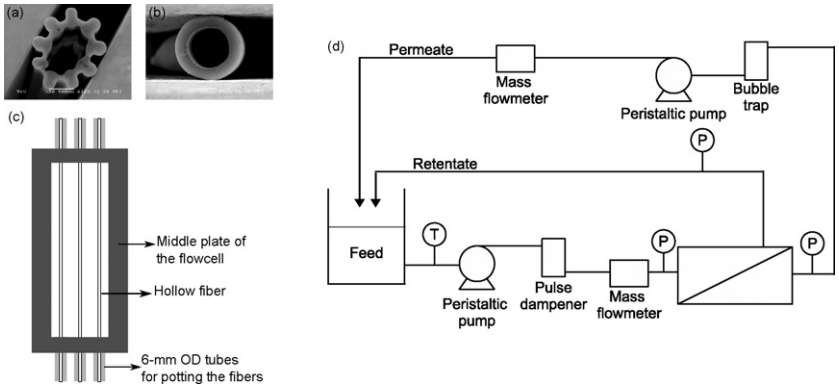

Fig. 2. SEM images of (a) the structured fiber and (b) the round fiber. (c) Drawing of the middle plate of the flowcell used in DVO experiments. (d) Schematic of the filtration setup.

settling of the particles. The pulse dampener on the feed side was used only in experiments with silica colloids because yeast particles would settle inside the pulse dampener. The bubble trap on the permeate side was used to prevent degassing products from affecting the permeate flux setpoint and measurement.

2.3. Direct-visual observation (DVO) experiments

The direct-visual observation experiments were done in a setup similar to that used in flux-cycling experiments. Instead of computer-logging of the data, feed and permeate flowrates and the permeate pressure were manually checked several times during the experiment. A permeate flux of 55 L/h m^2 and a Reynolds number of 120 was used.This *Re* corresponds to a lower velocity (11 mm/s) than that in the flux-cycling experiment modules as the hydraulic diameter was much larger in the flowcell. The permeate and retentate was recycled to the feed tank and each filtration was carried out for one hour. The surface of the membranes was observed with a NI 1744 Smart Camera (National Instruments) with a monochrome 1280 × 1024 CCD image sensor. The zoom system used (Optem Zoom 160, Qioptic Photonics) had a 2.0× objective lens and 1.0× dovetail tube, which allowed up to 16 times magnification with a 32 mm working distance. The resolution was 900 lp/mm or 1.11 μm and the depth-of-focus was 7 μm at the highest magnification. At the lowest magnification, the resolution was 54 lp/mm or 18.5 μm and the depth-of-focus was 1.75 mm. Illumination was done using fiber-optic bundles coaxially from behind the lens and outside, from above the observed area of the flow cell.

During filtration, 5 images with 1 s intervals were taken every 3 min. For the structured and twisted fibers, the zoomed area was switched manually from the bottom of the grooves and the top of the fins every 3 min, so that from each of these areas images were taken every 6 min. The images were analyzed to determine the fractional coverage of the membrane area with yeast particles using ImageJ.

A 0.005 wt% suspension of yeast cells in ultrapure water was used in the filtrations with DVO. The yeast cells were dyed with Coomassie® Brilliant Blue R-250 (Acros) according to the procedure used by Kang et al. [24]. 1 g of the as-purchased yeast was first diluted to 250 mL with ultrapure water and washed and centrifuged three times at 2500 rpm for 10 min, discarding the supernatant. The precipitated yeast was then dried and dispersed in a mixture of 0.15 g Brilliant Blue dye, 25 mL acetic acid, 62.5 mL isopropanol and 161.5 mL water. After mixing for 3 h, the suspension was again centrifuged three times at 2500 rpm for 10 min, discarding the supernatant and redispersing the precipitate in ultrapure water each time. The final precipitate was dried for 24 h under air flow.

3. Results and discussion

3.1. Flux-cycling experiments

The experiments were done under laminar conditions with Reynolds numbers of 120 and 400. The reason for choosing Reynolds number instead of the cross-flow velocity as the fixed variable while comparing the different fibers is because Reynolds and Schmidt numbers determine the Sherwood number, which is the dimensionless number that characterizes the mass transfer behavior in this kind of systems [10,25,26]. As the feed concentrations and Schmidt numbers for colloidal silica particles and yeast are not the same, we cannot directly compare the behavior of these two feeds at the same Reynolds number. However, for a single feed suspension, at fixed Reynolds number, we can compare the effect of the microstructure and twist in the fibers on the mass transfer.

As explained before in Section 2.2, to assess fouling reversibility we increase the permeate flux by 5 L/h m^2, then reduce it to the flux step before and compare the TMPs before and after the increased flux step. We must note here that assigning whether or not the fouling is reversible depends on the method used to reverse the particle deposition. Backwashing, increasing cross-flow or continuing cross-flow while stopping permeation are some of the ways that can be used to resuspend the particles on the membrane to the bulk [27–29]. The degree of reversibility depends on which method is used, and the intensity of the method, i.e. backwash flux, cross-flow velocity, etc. As the 5 L/h m^2 decrease in flux is only a mild relaxation, what is found to be irreversible fouling in these experiments can still be reversible with other methods mentioned before. However, it can distinguish between a loose, dynamic polarization layer and a stagnant cake [23,30].

3.1.1. Colloidal silica filtration

During the filtrations of the silica sol, for both Reynolds numbers, particle deposition started at a lower flux for both the structured and twisted fibers compared to the round fibers (Figs. 3 and 4). After this critical flux where the first particle deposition was observed by an increasing TMP, the particle deposition rate (as deduced from the dP/dt) was mostly higher for the twisted fiber compared to the structured fiber. On the other hand, although particle deposition took place earlier in the structured fiber compared to the round one, at fluxes higher than the critical flux, the rate of particle deposition was similar for the two fibers.

In the structured fibers, when the feed flow is parallel to the direction of the grooves in the fiber, within these grooves the shear rate will be lower than that on the fins. The result of this is that concentration polarization is more intense, which causes the particle deposition to start first within the grooves. Nevertheless, after

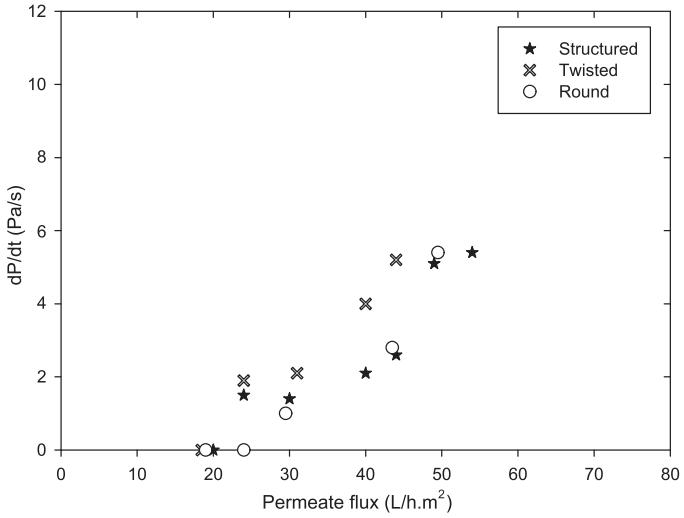

Fig. 3. Fouling rate during silica filtration at *Re* = 120.

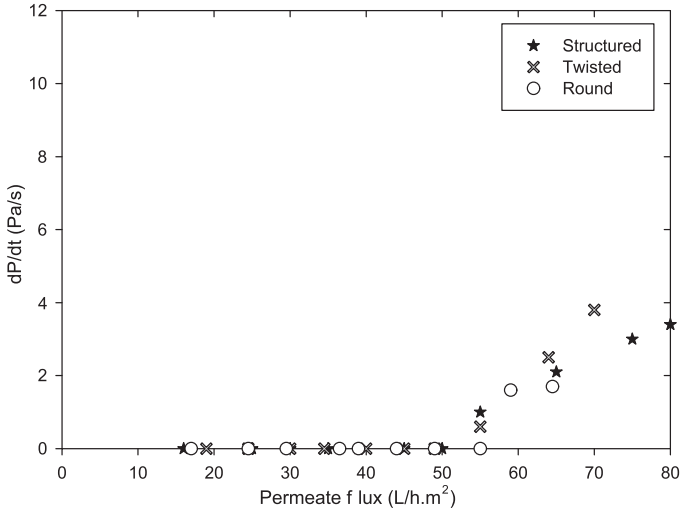

Fig. 4. Fouling rate during silica filtration at *Re* = 400.

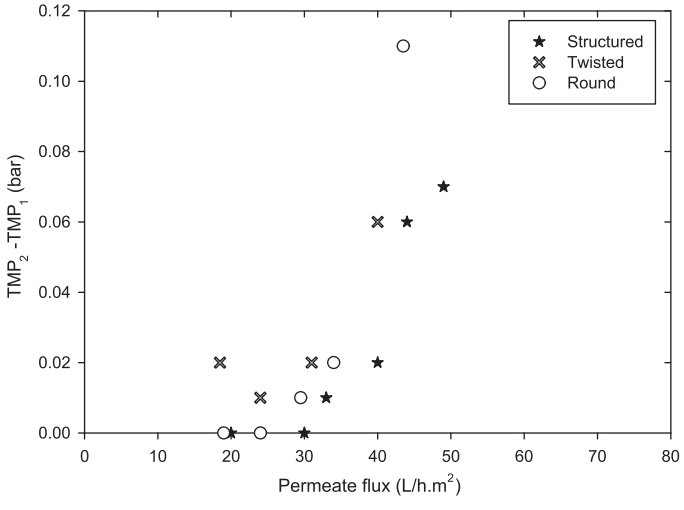

Fig. 5. Fouling irreversibility during silica filtration at *Re* = 120.

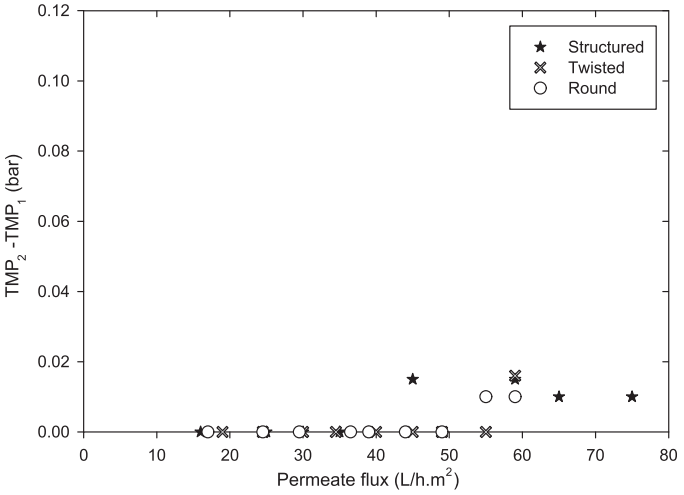

Fig. 6. Fouling irreversibility during silica filtration at *Re* = 400.

an initial deposition in the grooves, the deposition appears to be similar for the structured and round fibers.

At *Re* = 120, the twisted fibers foul faster and more irreversibly than the structured and round fibers (Figs. 3 and 5). In our previous studies, we observed inhomogeneous deposition of this silica sol on the structured fibers in dead-end filtrations and attributed this to the concentration profile in the thick polarization layers [31]. However, in cross-flow filtrations, the concentration polarization layers are expected to be much thinner. For the twisted fiber, due to the secondary flows that might result from the twisted surface one would expect more mixing and decreased concentration polarization. As will be explained in more detail later, at low *Re* only corner vortices form while after a critical *Re* these turn into Dean vortices, which are more effective in depolarizing the particle buildup [32]. If the effect of the secondary flow is little, then in the grooves of the twisted fibers it may only be able to homogenize the present concentration polarization layer without carrying particles out of the groove and back to the bulk.

At *Re* = 120, the critical flux for irreversibility is significantly higher than the critical flux for particle deposition for the structured fibers unlike for the twisted and round fibers (Fig. 11). Although particle deposition starts in the grooves, when the flux is lowered, more of the permeate would flow towards the fins due to the higher resistance in the grooves. This balancing between the different local fluxes through the fins and the grooves can keep the fouling appear reversible until a similar deposit forms on the fins.

At *Re* = 400, although some irreversibility is observed for all three fibers, the TMP differences remain lower than 0.01 bar for the whole flux range, which is close to the detection limit of the pressure sensors (0.005 bar) (Fig. 6).

3.1.2. Yeast filtration

During the filtrations of the yeast suspension, there is a clear difference between the fouling behavior of structured and twisted fibers (Figs. 7–10). At both Reynolds numbers, both the critical flux for particle deposition and for irreversibility are higher for the twisted fiber. The particle deposition rate is similar for twisted and round fibers, except for fluxes higher than 40 L/h m^2 at *Re* = 120. On the other hand, for the structured fiber, the particle deposition is faster at both *Re* throughout the whole flux range. Twisting the structured fibers also improves the reversibility of particle deposition, as at both Reynolds numbers, the critical flux for irreversible deposition is highest on the twisted fibers (Fig. 12).

At *Re* = 120, the degree of irreversibility is significantly higher on the structured fiber compared to the twisted and round fibers. For

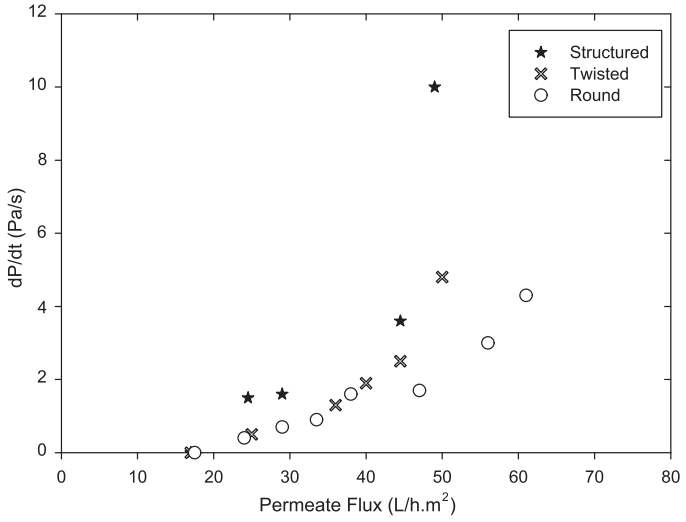

Fig. 7. Fouling rate during yeast filtration at *Re* = 120.

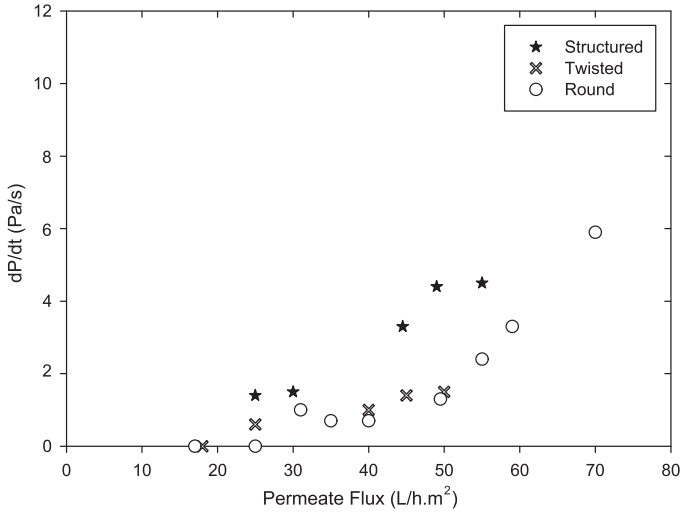

Fig. 8. Fouling rate during yeast filtration at *Re* = 400.

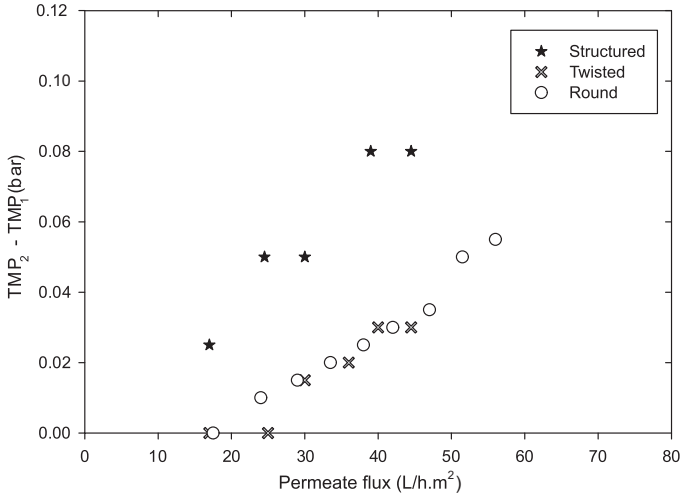

Fig. 9. Fouling irreversibility during yeast filtration at *Re* = 120.

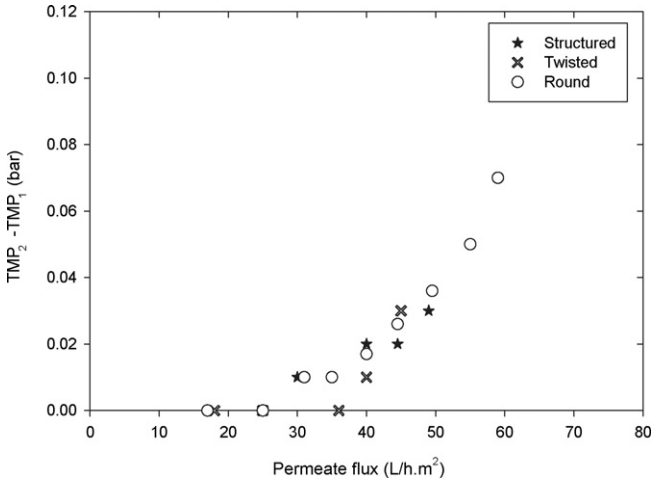

Fig. 10. Fouling irreversibility during yeast filtration at *Re* = 400.

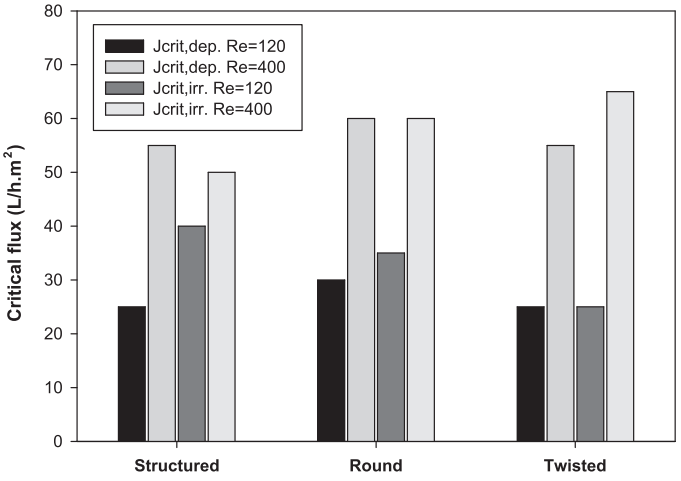

Fig. 11. Critical flux for particle deposition and irreversibility for silica filtration.

these latter fibers it is mostly similar after their critical fluxes for irreversible deposition. Increasing the Reynolds number improves the fouling reversibility for all the fibers (Fig. 12).

Increasing the Reynolds number from 120 to 400 increases the critical fluxes about two-fold for all three fibers during silica filtration (Fig. 11). During yeast filtration the critical flux is affected much less or not affected at all (Fig. 12). For the structured and twisted fibers, the critical flux for particle deposition during yeast filtration is 25 L/h m^2 at both *Re* and for the round fiber it only increases from 25 L/h m^2 to 30 L/h m^2 with increasing *Re*. Although the effect of Reynolds number on the critical flux for irreversibility is slightly more pronounced, it is still less than its effect during silica filtrations. Particle deposition rates and the degree of irreversibility with increasing flux are less at the higher Reynolds number. However, the critical fluxes where particle deposition first occurs (and is irreversible) are quite low in all cases of yeast filtration. This behavior is probably due to the stronger adsorption of yeast particles on the membrane [24,33]. On the other hand, considering the particle deposition rate and reversibility of deposition, twisting the structured fibers results in a clear improvement during yeast filtration, while during silica filtration the differences between all three fibers is much less.

For the colloidal silica particles, the main depolarization mechanism is the entropic back-diffusion [4]. In our previous study, we showed that in the absence of cross-flow the concentration polarization layers with silica colloids can be as thick as the size of

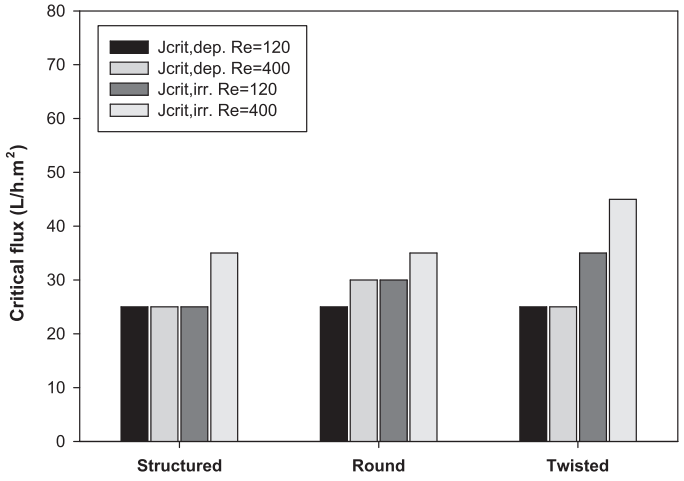

Fig. 12. Critical flux for particle deposition and irreversibility for yeast filtration.

the convolutions in the structured fibers and this can give rise to inhomogeneous deposition patterns on the structured fibers [31]. Although under the cross-flow conditions used here, the concentration polarization layers are thinner and probably do not create such inhomogeneous deposition patterns, they can still have significant resistance. The improvement in critical flux obtained with increasing Reynolds number for the silica filtrations is considered to be because increasing cross-flow suppresses polarization and therefore delays fouling.

For the micron-sized yeast particles, electrostatic repulsion and shear-induced diffusion are the main depolarization mechanisms [4,24,34]. The high shear-induced diffusivity can create a very thick concentration polarization layer. However the resistance of this layer would be very low (which can be deduced from the Kozeny–Carman relation or the low osmotic pressure), so the effect of the polarization layer would not be significant. In yeast filtrations, fouling starts to occur at low fluxes due to adsorption on the membrane surface. However, after the deposition of the first layer due to adsorption, the rate and reversibility of further deposition depends on the interactions between yeast particles. Considering the whole flux range including fluxes higher than the critical flux, increasing shear decreases the particle deposition rates and the irreversibility of the deposit.

The difference between the structured and twisted fibers during yeast filtrations is attributed to secondary flows induced by the twisting. In general, when the flow direction is not parallel to the solid surface, the imbalance between viscous forces and centrifugal forces originating from the curvature of the surface creates secondary flows and forms vortices in the fluid. These vortices, which are called corner vortices or Ekman cells at low *Re* and Dean vortices after a critical *Re*, have been used to decrease concentration polarization in membrane processes and to improve mixing in microfluidic channels [14–16,32,35–37]. For the twisted fiber, although we do not have a fully coiled or helical channel, the twisting of the corrugations creates a helical half-channel. The Dean numbers calculated for *Re* = 120 and 400 are 4 and 14, respectively. A critical Dean number below which Dean vortices do not occur has been identified by several authors [14,15]. On the other hand, Moulin et al. have shown that secondary flows occur even at very low Dean numbers, although they might not have clearly observable effects in the mass transfer [38]. Mallubhotla et al. suggest that in helical channels, the critical condition where the secondary flow pattern changes from a single pair of counter-rotating corner vortices to two pairs of vortices, which are called Dean vortices, depends on two dimensionless quantities, namely the Dean number and the Germano number [15]. According to the criteria they

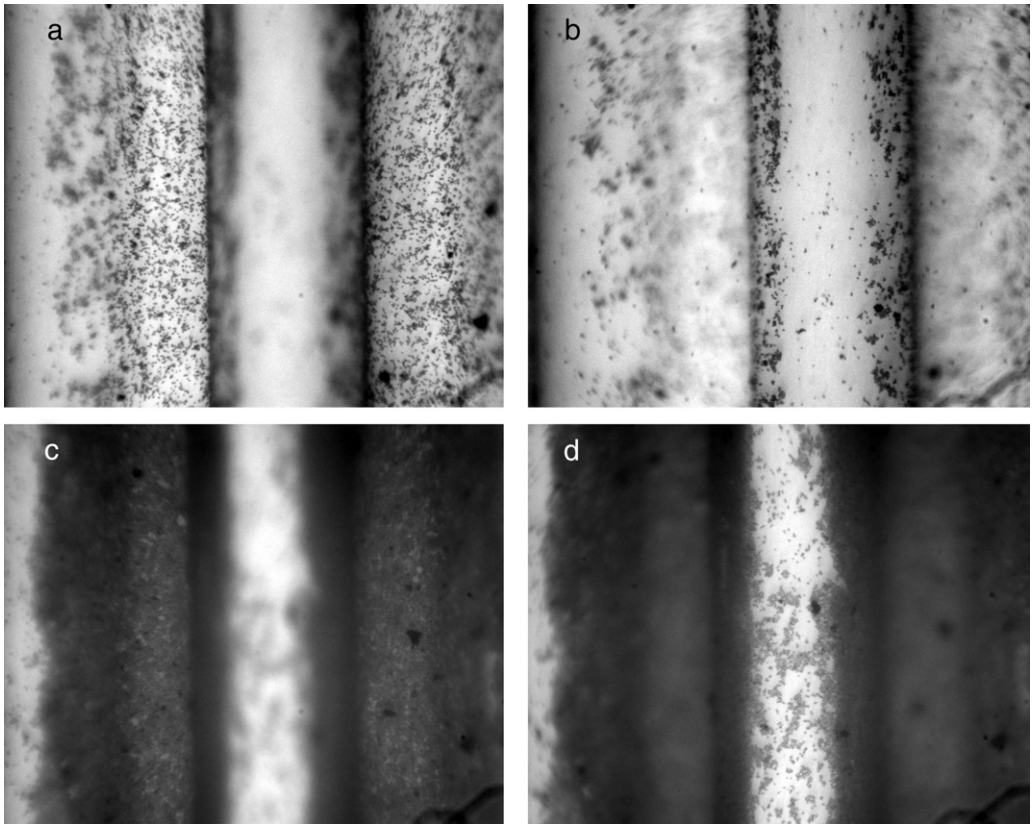

Fig. 13. Images of the structured fiber surface during filtration of the yeast suspension. Bottom of grooves (a) after 9 min and (c) after 57 min. Top of fins (b) after 6 min and (d) after 60 min.

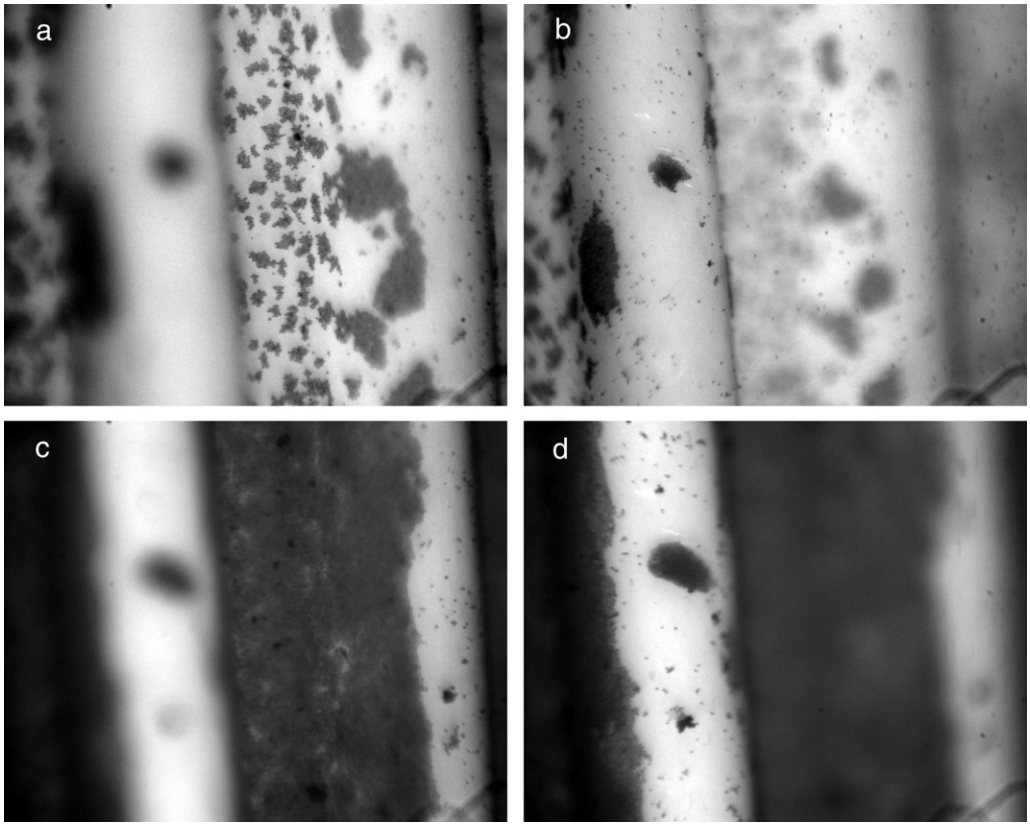

Fig. 14. Images of the twisted fiber surface during filtration of the yeast suspension. Bottom of grooves (a) after 9 min and (c) after 57 min. Top of fins (b) after 6 min and (d) after 60 min.

suggest, if we would assume that in the half channels of the twisted fiber same criteria would hold as in twisted tubes of the same dimensions, at $Re = 400$ Dean vortices might form. Although it is difficult to say if this actually happens or not, even in the case of corner vortices that form due to the twisting, the higher shear rates and shear rate gradients can affect the back diffusion of yeast particles. Also recently, Rusconi et al. observed the formation of biofilm streamers in curved microfluidic channels during laminar flow with very low Reynolds numbers (0.02–0.1), which did not appear in straight channels [39]. With numerical simulations, they showed the formation of a secondary flow consisting of two symmetrical counter-rotating vortices in the proximity of the corners. While in the experimental conditions of their work, the Reynolds and Dean numbers were even smaller than those in ours, the occurence of secondary flows and their effect on the formation of biofilms were clearly illustrated.

3.2. Direct visual observation of yeast deposition

From the images taken during yeast filtration, it is observed that for both structured and twisted fibers the particle deposition rate is lower on the fins (Figs. 13(b), (d) and 14(b), (d)). This can be attributed to the higher shear rate on the fins, which allows less deposition. On the twisted fibers, the deposition rate on the fins is even lower than that of the structured fiber. Also, the particles appear to deposit in patches both in the grooves and on the fins on the twisted fiber, whereas on the structured fiber and the round fiber (images not shown here) the particles appear more randomly distributed over the whole surface. This aggregation can be due to the shear induced by secondary flows due to the twist [40–42]. It can also explain the better reversibility of fouling for the twisted fibers observed during the flux-cycling experiments, as clusters of particles are more easily swept away by the cross-flow as compared to individual particle deposits [27,43]. This patchy deposition and the observation that on the fins of the twisted fibers there is less overall deposition is attributed to secondary flows forming due to the twist in the fiber surface.

Analysis of the images taken during filtration reveal that the particle deposition rate in the grooves of the structured and twisted fibers and that on the round fiber are similar (Fig. 15). This seems unexpected at first thought, as the shear rate on the round fiber surface is similar to the shear rate on the fins of the structured fibers, which is higher than that in the grooves. Furthermore, even at Reynolds numbers as low as 10, on structured and twisted fibers

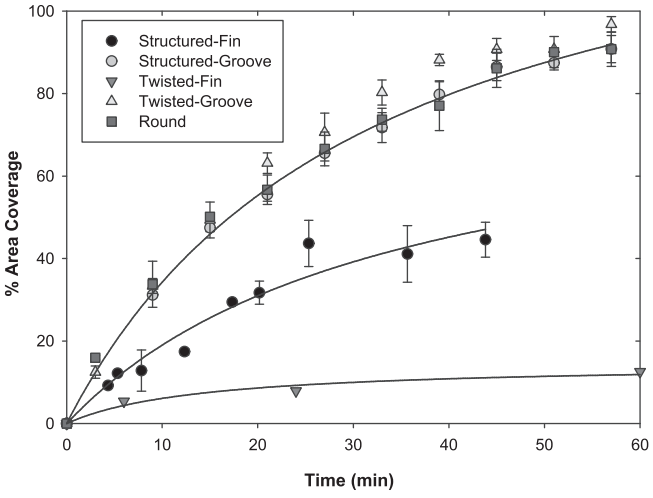

Fig. 15. % Area coverage in time during yeast filtration.

the deposition rate on the fins was observed to be lower than that within the grooves. As the grooves fill up in time, the deposition advances towards the fins from the sides towards the top. In dead-end filtrations, a homogeneous deposition was observed on fins and grooves. This can be explained by the shear-induced migration of particles in concentrated suspensions from high to low shear rate regions [34,44]. For the round fibers the shear rate gradient is from the surface of the fiber towards the bulk. On the other hand, for the structured fibers the shear rate also increases from the grooves towards the fins and for the twisted fibers it varies within the vortices. In addition to the shear rate gradients, Kim et al. suggest that in suspensions under shear, particles also migrate due to curvature in the radially outward direction, which can also cause less particle deposition on the fins of the structured and twisted fibers [45].

4. Conclusions

The fouling behavior of microstructured hollow fiber membranes was investigated in cross-flow filtrations of colloidal silica and yeast. These microstructured fibers were compared to round fibers with the same intrinsic properties. Also the effect of twisting the microstructured fibers around their own axes on the particle deposition is investigated. During silica filtrations, the three different fibers showed similar behavior and increasing Reynolds number increased the critical fluxes significantly. During yeast filtrations, the twisted fiber performed better than the structured fiber and similar to the round fiber. Among the three fibers, during yeast filtrations the critical flux for irreversibility was highest for the twisted fiber. The Reynolds number had little effect on the critical fluxes for particle deposition, which was attributed to the strong adsorption of yeast particles on the membrane. On the other hand, the critical fluxes for irreversibility increased with increasing Reynolds number for all three fibers. In direct visual observation experiments using yeast particles, we observed that on the fins of the structured and twisted fibers, the initial deposition rate is much lower than that in the grooves. This is mainly attributed to the shear-induced migration of the yeast particles from areas of high shear (fins) to those of low shear (grooves). Furthermore, the particle deposition rate on the fins of the twisted fiber was lower than that on the fins of the structured fiber. This observation, together with the observed high critical fluxes for the twisted fiber led to the conclusion that the twisted surface promotes secondary flows. These secondary flows can depolarize the buildup of micron-sized yeast particles since the diffusion of these particles are highly effected by gradients in shear rate. On the other hand, as shear-induced diffusion is not significant for the smaller silica colloids twisting does not have an improving effect on filtration.

References

[1] N. Hilal, O.O. Ogunbiyi, N.J. Miles, R. Nigmatullin, Methods employed for control of fouling in mf and uf membranes: a comprehensive review, Separation Science and Technology 40 (2005) 1957–2005.
[2] D. Rana, T. Matsuura, Surface modifications for antifouling membranes, Chemical Reviews 110 (2000) 2448–2471.
[3] H.B. Winzeler, G. Belfort, Enhanced performance for pressure-driven membrane processes: the argument for fluid instabilities, Journal of Membrane Science 80 (1993) 35–48.
[4] P. Bacchin, D. Si-Hassen, V. Starov, M.J. Clifton, P. Aimar, A unifying model for concentration polarization, gel-layer formation and particle deposition in cross-flow membrane filtration of colloidal suspensions, Chemical Engineering Science 57 (2002) 77–91.
[5] D.M. Krstic, M.N. Tekic, M.D. Caric, S.D. Milanovic, The effect of turbulence promoter on cross-flow microfiltration of skim milk, Journal of Membrane Science 208 (2002) 303–314.
[6] Z.F. Cui, S. Chang, A.G. Fane, The use of gas bubbling to enhance membrane processes, Journal of Membrane Science 221 (2003) 1–35.
[7] J.A. Howell, R.W. Field, D. Wu, Yeast cell microfiltration: flux enhancement in baffled and pulsatile flow systems, Journal of Membrane Science 80 (1993) 59–72.
[8] J. Balster, M.H. Yildirim, D.F. Stamatialis, R.G.H. Ibanez, R. Lammertink, V. Jordan, M. Wessling, Morphology and microtopology of cation-exchange polymers and the origin of the overlimiting current, Journal of Physical Chemistry B 111 (2007) 2152–2165.
[9] K. Scott, A.J. Mahmood, R.J. Jachuck, B. Hu, Intensified membrane filtration with corrugated membranes, Journal of Membrane Science 173 (2000) 1–16.
[10] N. Tzanetakis, K. Scott, W.M. Taama, R.J. Jachuck, Mass transfer characteristics of corrugated surfaces, Applied Thermal Engineering 24 (2004) 1865–1875.
[11] M.J. van der Waal, S. Stevanovic, I.G. Racz, Mass transfer in corrugated-plate membrane modules. ii. Ultrafiltration experiments, Journal of Membrane Science 40 (1989) 261–275.
[12] L.-Z. Zhang, Convective mass transport in cross-corrugated membrane exchangers, Journal of Membrane Science 260 (2005) 75–83.
[13] M.E. Brewster, K.-Y. Chung, G. Belfort, Dean vortices with wall flux in a curved channel membrane system. 1. A new approach to membrane module design, Journal of Membrane Science 81 (1993) 127–137.
[14] J.N. Ghogomu, C. Guigui, J.C. Rouch, M.J. Clifton, P. Aptel, Hollow-fibre membrane module design: comparison of different curved geometries with dean vortices, Journal of Membrane Science 181 (2001) 71–80.
[15] H. Mallubhotla, S. Hoffmann, M. Schmidt, J. Vente, G. Belfort, Flux enhancement during dean vortex tubular membrane nanofiltration. 10. Design, construction and system characterization, Journal of Membrane Science 141 (1998) 183–195.
[16] H. Mallubhotla, E. Nunes, G. Belfort, Microfiltration of yeast suspensions with self-cleaning spiral vortices: possibilities for a new membrane module design, Biotechnology and Bioengineering 48 (1995) 375–385.
[17] L. Broussous, J.C. Ruiz, A. Larbot, L. Cot, Stamped ceramic porous tubes for tangential filtration, Separation and Purification Technology 14 (1998) 53–57.
[18] L. Broussous, P. Schmitz, H. Boisson, E. Prouzet, A. Larbot, Hydrodynamic aspects of filtration antifouling by helically corrugated membranes, Chemical Engineering Science 55 (2000) 5049–5057.
[19] P.Z. Çulfaz, E. Rolevink, C.J.M. van Rijn, R.G.H. Lammertink, M. Wessling, Microstructured hollow fibers for ultrafiltration, Journal of Membrane Science 347 (2009) 32–41.
[20] P. Bacchin, P. Aimar, R.W. Field, Critical and sustainable fluxes: theory, experiments and applications, Journal of Membrane Science 281 (2006) 42–69.
[21] S. Metsamuuronen, J. Howell, M. Nystrom, Critical flux in ultrafiltration of myoglobin and baker's yeast, Journal of Membrane Science 196 (2002) 13–25.
[22] D. Wu, J.A. Howell, R.W. Field, Critical flux measurement for model colloids, Journal of Membrane Science 152 (1999) 89–98.
[23] V. Chen, A.G. Fane, S. Madaeni, I.G. Wenten, Particle deposition during membrane filtration of colloids: transition between concentration polarization and cake formation, Journal of Membrane Science 125 (1997) 109–122.
[24] S.-T. Kang, A. Subramani, E.M.V. Hoek, M.A. Deshusses, M.R. Matsumoto, Direct observation of biofouling in cross-flow microfiltration: mechanisms of deposition and release, Journal of Membrane Science 244 (2004) 151–165.
[25] P. Pradanos, J.I. Arribas, A. Hernandez, Mass trans-fer coefficient and retention of pegs in low pressure cross-flow ultrafiltration through asymmetric membranes, Journal of Membrane Science 99 (1995) 1–20.
[26] F.P. Incropera, D.P. DeWitt, Fundamentals of Heat and Mass Transfer, Wiley, New York, 2002.
[27] H. Li, A.G. Fane, H.G.L. Coster, S. Vigneswaran, Observation of deposition and removal behaviour of submicron bacteria on the membrane surface during crossflow microfiltration, Journal of Membrane Science 217 (2003) 29–41.
[28] Y. Marselina, P. Lifia, R.M. Le-Clech, V. Chen, Characterisation of membrane fouling deposition and removal by direct observation technique, Journal of Membrane Science 341 (2009) 163–171.
[29] W.D. Mores, R.H. Davis, Yeast-fouling effects in cross-flow microfiltration with periodic reverse filtration, Industrial and Engineering Chemistry Research 42 (2003) 130–139.
[30] Y. Bessiere, N. Abidine, P. Bacchin, Low fouling conditions in dead-end filtration: evidence for a critical filtered volume and interpretation using critical osmotic pressure, Journal of Membrane Science 264 (2005) 37–47.
[31] P. Çulfaz, S. Buetehorn, L. Utiu, M. Kueppers, B. Bluemich, T. Melin, M. Wessling, R.G.H. Lammertink, Fouling behavior of microstructured hollow fiber membranes in dead-end filtrations: critical flux determination and nmr imaging of particle deposition, Langmuir, doi:10.1021/la1037734.
[32] H. Fellouah, C. Castelain, A. Ould El Moctar, H. Peerhossaini, A criterion for detection of the onset of dean instability in newtonian fluids, European Journal of Mechanics B: Fluids 25 (2006) 505–531.
[33] S. Wang, G. Guillen, E.M.V. Hoek, Direct observation of microbial adhesion to membranes, Environmental Science and Technology 39 (2005) 6461–6469.
[34] G. Belfort, R.H. Davis, A.L. Zydney, The behavior of suspensions and macromolecular solutions in crossflow microfiltration, Journal of Membrane Science 96 (1994) 1–58.
[35] M. Lopez, M. Graham, Enhancement of mixing and adsorption in microfluidic devices by shear-induced diffusion and topography-induced secondary flow, Physics of Fluids 20 (2008) 053304.
[36] A.D. Stroock, S.K. Dertinger, A. Ajdari, I. Mezic, H.A. Stone, G.M. Whitesides, Chaotic mixer for microchannels, Science 295 (2002) 647–651.
[37] A.D. Stroock, S.K. Dertinger, G.M. Whitesides, A. Ajdari, Patterning flows using grooved surfaces, Analytical Chemistry 74 (2002) 5306–5312.
[38] P. Moulin, P. Manno, J.C. Rouch, C. Serra, M.J. Clifton, P. Aptel, Flux improvement by dean vortices: ultrafiltration of colloidal suspensions and macromolecular solutions, Journal of Membrane Science 156 (1999) 109–130.

[39] R. Rusconi, S. Lecuyer, L. Guglielmini, H.A. Stone, Laminar flow around corners triggers the formation of biofilm streamers, Journal of the Royal Society 7 (2010) 1293–1299.
[40] Y. Kikuchi, H. Yamada, H. Kunimori, T. Tsukada, M. Hozawa, C. Yokoyama, M. Kubo, Aggregation behavior of latex particles in shear flow confined between two parallel plates, Langmuir 21 (2005) 3273–3278.
[41] P. Stamberger, The mechanical stability of colloidal dispersions, Journal of Colloid Science 17 (1962) 146–154.
[42] D.L. Swift, S.K. Friedlander, The coagulation of hydrosols by brownian motion and laminar shear flow, Journal of Colloid Science 19 (1964) 621–647.
[43] Y.P. Zhang, A.G. Fane, A.W.K. Law, Critical flux and particle deposition of fractal flocs during crossflow microfiltration, Journal of Membrane Science 353 (2010) 28–35.
[44] R.J. Phillips, R.C. Armstrong, R.A. Brown, A.L. Graham, J.R. Abbott, A constitutive equation for concentrated suspensions that accounts for shear-induced particle migration, Physics of Fluids A 4 (1992) 30–40.
[45] J.M. Kim, S.G. Lee, C. Kim, Numerical simulations of particle migration in suspension flows: Frame-invariant formulation of curvature-induced migration, Journal of Non-Newtonian Fluid Mechanics 150 (2008) 162–176.